Extracting Dynamical Models from Data

Michael F. Zimmer zim@neomath.com

October 28, 2021

Abstract

The FJet approach is introduced for determining the underlying model of data from a dynamical system. It borrows ideas from the fields of Lie symmetries as applied to differential equations (DEs), and numerical integration (such as Runge-Kutta). The technique can be considered as a way to use machine learning (ML) to derive a numerical integration scheme. The technique naturally overcomes the "extrapolation problem", which is when ML is used to extrapolate a model beyond the time range of the original training data. It does this by doing the modeling in the phase space of the system, rather than over the time domain. When modeled with a type of regression scheme, it's possible to accurately determine the underlying DE, along with parameter dependencies. Ideas from the field of Lie symmetries applied to ordinary DEs are used to determine constants of motion, even for damped and driven systems. These statements are demonstrated on three examples: a damped harmonic oscillator, a damped pendulum, and a damped, driven nonlinear oscillator (Duffing oscillator). In the model for the Duffing oscillator, it's possible to treat the external force in a manner reminiscent of a Green's function approach. Also, in the case of the undamped harmonic oscillator, the FJet approach remains stable approximately 10⁹ times longer than 4th-order Runge-Kutta.

1 Introduction

This paper is concerned with modeling data that arises from a dynamical system. Specifically, the focus is on using machine learning (ML) for the modeling, with the hope of converting that model into something more insightful, such as a differential equation (DE) and accompanying domain knowledge (such as constants of motion). This endeavor is broken down into these five goals:

- 1. Extrapolate model beyond training data times.
- 2. Determine underlying DE.
- 3. Determine parameter dependencies in DE.
- 4. Estimate stability/accuracy of model.
- 5. Determine related domain knowledge.

Related Work

Previous work of interest has to do with modeling the (nonlinear) dynamics of a system, given time series information from measurements. Since the subfield of interest to this paper is also on understanding the underlying dynamics, curve fitting procedures such as time series analysis will not be reviewed as related work.

While previous work really may be traced back to attempts at modeling physical systems, such as by Poincaré [1885] with his work on celestial mechanics (also see [Holmes, 1990], Poincaré [1993]), modern work might be identified as beginning with Packard et al. [1980] in their study of the time series of nonlinear and chaotic time series, and the study by Takens [1981] on turbulence. Not long after this, the work by Crutchfield and McNamara [1987] produced a form of analysis that would be repeated: the data was fit to a model of the form dy/dt=F, where the choice of F was guided by minimizing a complexity measure. They considered general dynamical systems, and in particular the examples of the Lorenz model and the Duffing oscillator. A number of other significant works would soon follow, including [Broomhead and Lowe, 1988], [Casdagli, 1989], [Cremers and Hübler, 1987], [Breeden and Hübler, 1990], [Gouesbet, 1992], and others. The techniques that were used in this time period for modeling F(y) included polynomial expansions, radial basis functions, neural nets (NNs), B-splines, etc; the reader is referred to the review by Aguirre and Letellier [2009] for a more complete discussion.

This problem has recently been receiving renewed attention, often with a focus on NN techniques. The common theme has been to enforce a physics prior onto the network, forcing it to obey conserved dynamics. For example, [Lutter et al., 2019] introduced a Lagrangian prior and modeled robot tracking control. This Lagrangian technique was generalised by [Cranmer et al., 2020], who considered non-dissipative applications of a double pendulum, relativistic particle, and a 1D wave equation. Also, [Greydanus et al., 2019] used a Hamiltonian prior on a NN and studied conservative systems such as a mass-spring system and a pendulum (ideal and real data). [Toth et al., 2019] introduced Hamiltonian Generative Networks to model conserved densities satisfying Hamiltonian dynamics, which has applications towards image analysis, for example.

The work of [Rudy et al., 2017] also begins with a regularized to dy/dt = F, but in this case software (SINDy) was used to help search the function space for useful features. They applied this technique to the Navier-Stokes equation, the quantum harmonic oscillator, the diffusion equation, and other PDEs Also, Liu et al. [2021] have found how to use NNs to detect the presence of, and model, non-conservative forces in a physics context. Finally, there are other contributions besides these, but space does not permit a more complete review.

Outline

The layout of the paper is that of an Overview (Section 2), three Examples (Section 3, 4, and 5), Final Remarks (Section 6), and three Appendices.

The Overview covers background for the FJet method. It covers the scope of dynamical systems being considered here, the basic idea of the FJet modeling, recommendations

for choosing the variables and model, and also how to compute constants of motion making use of ideas from Lie symmetries applied to DEs. The three Examples are on: damped harmonic oscillator, damped pendulum, and the Duffing oscillator. Their treatments largely follow the same logical progression, as an aid to the reader. After the Final Remarks, there are three Appendices, covering the Runge-Kutta scheme, stability of the harmonic oscillator, and a computation of the integration constant r, which in this case generalizes the energy for a *damped* harmonic oscillator.

2 Overview of FJet Approach

In this section the key issues of the problem and an outline of the solution are discussed.

2.1 Scope of Dynamical Systems

In this paper, the emphasis is on modeling a deterministic system from noisy observations. Specifically, the dynamical systems of interest in this paper will be those describable by an explicit ordinary DE (ODE) of the form

$$u^{(n)} = G(t, u, u^{(1)}, ..., u^{(n-1)})$$
(1)

where the superscript on u denotes the derivative with respect to the independent variable t. It is also convenient to define the function

$$\mathcal{D}(t, u, u^{(1)}, \dots, u^{(n)}) = u^{(n)} - G \tag{2}$$

so that solutions to the ODE can be understood 1 as being constrained to the surface $\mathcal{D}=0$.

Admittedly, the space of solutions allowed by this meager restriction (Eq. 1) is still vast and complex. In practice, the focus for now will be on equations where G is a sum of terms, each local and without singularities. An explicit dependence on the independent variable t is allowed, but the most successful modeling of such a system will occur when said dependence occurs through a function such as p(t) (which is well-approximated by a truncated Taylor series expansion, and also ideally has a bounded range of values). In that scenario, the values of p, \dot{p} , ... are collected with the training data, a model is built including the variables p, \dot{p} , ..., and the extrapolation solution is created from another p(t) (not necessarily the same as the one used in training). Since the solution is built upon a general external function p(t), it is similar to a Green's function approach.

2.2 Mapping Approach

In typical ML approaches for modeling dynamical systems, one is given training data over some finite time interval, and then after modeling seeks to make predictions over later times. Attempting to use an ML model beyond the domain of the training data is in general a problem for ML, since most ML models essentially work by interpolation. A simple illustration of this problem is afforded in Fig. 1 superimposed with a function

Said more precisely [Hydon, 2000], one should define the "lift" of a solution u=g(t) as $(t,g,g^{(1)},\ldots,g^{(n)})$ as the element that lies in the surface $\mathcal{D}=0$.

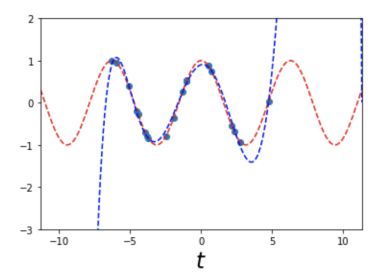


Figure 1: Extrapolation from fitting a polynomial to a few points from a sinusoid. The original function is shown in light red. Notice how outside the domain where training data was available (i.e., the interval $(-2\pi, 2\pi)$), the polynomial fit diverges from the true function.

 2 learned through polynomial regression fit to the data points in the interval $(-2\pi, 2\pi)$). In this example, the data is generated by sampling an underlying sine curve, but the polynomial fit to it will not assume this knowledge. As is clear from the figure, it makes an excellent fit to the data within the domain of training times, but it would obviously be ill-advised to use the model outside this interval.

To overcome this problem and be able to extrapolate a model beyond the training data for dynamical systems, the system is instead viewed with respect to its phase space. For systems with no explicit time dependence, the training data will exist in this space, and not require an additional time axis. For example, the phase space plot for a system such as a harmonic oscillator would reveal a time-parametrized orbit. Fig. 2 depicts such an orbit, illustrating how the current values of (u,\dot{u}) get updated by $(\Delta u,\Delta\dot{u})$ after the time increases from t to $t+\epsilon$. These changes are simply defined as

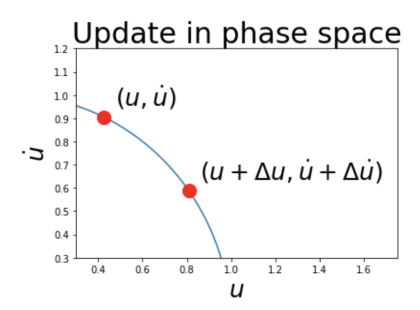


Figure 2: Points in phase space at t and $t + \epsilon$.

$$\Delta u = u(t + \epsilon) - u(t) \tag{3a}$$

$$\Delta \dot{u} = \dot{u}(t + \epsilon) - \dot{u}(t) \tag{3b}$$

²The trial form for the ML algorithm (polynomial regression with features $\{t^n|n\in\{0,1,...,6\}\}$) is admittedly a poor function for this. It is used only to make a point by creating a generic figure.

In this approach, the challenge is how to model these updates as a function of (u, \dot{u}) . Two separate models will be used: h_1 and h_2 ; they are referred to collectively as $h = (h_1, h_2)$.

$$\Delta u = h_1(u, \dot{u}) \tag{4a}$$

$$\Delta \dot{u} = h_2(u, \dot{u}) \tag{4b}$$

(Note that in these equations, u and \dot{u} are measured at t.) More generally, the model h will relate 3 the set of predictor variables X to the response variables Y via Y=h(X). In this example, $X=\{u,\dot{u}\}$ and $Y=\{\Delta u,\Delta\dot{u}\}$. At this point, any relevant ML technique to learn h can be used, from NNs to a regression model. When that has been accomplished, the remaining task is to perform the extrapolation, which is easily done via an algorithm such as Algo. 1 This will be called a *generative* algorithm, since it

Algorithm 1: Generative Algorithm

```
Input: t_0, N
Init: t = t_0
Init: u = u(t)
Init: \dot{u} = \dot{u}(t)
for i = 0 to N do

tmp_h_1 = h_1(u, \dot{u})
tmp_h_2 = h_2(u, \dot{u})
u \leftarrow u + \text{tmp}_h_1
\dot{u} \leftarrow \dot{u} + \text{tmp}_h_2
t \leftarrow t + \epsilon
print(u, t)
end for
```

generates u(t) from the learned ML model h. It's important that the same time step (ϵ) that is used in the data collection also be used in the generative step; this is because the models will in general be nonlinear functions of it. Also, the algorithm as explained here is only for 2nd-order, non-driven systems. However, it can be easily extended to those cases by using additional tmp_ variables, as will be done in Sec. 5.

2.3 Jet Space

For autonomous systems described by a second order DE, it is enough to do the modeling in the phase space (u,\dot{u}) . For systems described by a higher order DE, higher derivatives of u are needed, and thus the need for the associated jet space becomes apparent [cf. Sec. 2.3 in Olver, 1993]. Suppose the underlying space of the system is $Q\times U$, where Q represents the independent variables and U represents the dependent variables. Now define $U^{(n)}$, the nth-order prolongation of U, as the set of all possible derivatives of variables in U with respect to variables in Q, up to the nth-order. Thus, the nth-order jet space of $Q\times U$ is $\mathcal{J}^{(n)}=Q\times U^{(n)}$. As an example, taking $U=\{u\}$ and $Q=\{x,t\}$,

 $^{^{3}}$ Different models and even different predictor variables can be used when modeling each member of Y.

the second prolongation ⁴ of U is $U^{(2)} = (u; u_x, u_t; u_{xx}, u_{xt}, u_{tt})$, and its 2nd-order jet space is $\mathcal{J}^{(2)} = (x, t) \times U^{(2)}$.

2.4 Modeling

There are a number of available options with respect to model and variable choices. If the goal is only to model h(X) as accurately as possible, without regard to interpretability or deriving the underlying DE, then any function approximation technique can be used for h(X). Examples include, but are not limited to, neural nets (NNs), boosting algorithms, random forest regressors, regression, etc. However, if the goal is to determine the underlying DE and understand its composition, then it is recommended to use something here named *feature regression*.

Feature regression is a form of regression, differing from usual regression in that the variables are not a selection of the *independent* variables, but rather of the *jet space* variables. The model is expressed as

$$h(X) = a_0 f_0 + a_1 f_1 + a_2 f_2 + \cdots$$
 (5)

where the a_i are scalars and the f_i are functions of $\mathcal{J}^{(n-1)}$ (for an nth-order DE) and are called "features". Typically these features will be low-order monomials (or functions thereof), or possibly trigonometric functions. The features will be local functions, but in principle may include non-local terms as well. In other works, similar types of models go by other names. For example, in ML/Stats there are the *functionally additive models* (*FAMs*); in earlier work on extracting models from data, such models were called a *linear in the parameter model* [Aguirre and Letellier, 2009]. It also bears some degree of similarity with the results of *symbolic regression*, although not the searching procedure used therein.

If one has made the choice of using feature regression, the next step is to select the functions f_i . It will be shown in Appendix A that this choice is not an arbitrary decision. In fact, for a given level of accuracy in ϵ (where ϵ is the time step), the choice is specific. Of course, with unknown dynamics, one can't rely on the approach of Appendix A, but one is still able to rely on the modeling procedure to identify the relative importance of the features. This happens naturally in the course of modeling [Hastie et al., 2009], with coefficients either being set to zero or small values, or with their relative importance being produced.

It is important to consider all possible terms that might result from a well-behaved, low-order complexity model. With the results of Appendix A as a guide, the following generating function is offered as a rubric If \mathcal{F} is the original set of features, then the full set of *potential* features that should be considered are augmented as

$$\mathcal{F} \to \sum_{n=1} (\mathcal{F} + \partial_J \mathcal{F} + \partial_J \partial_J \mathcal{F} + \cdots)^n$$
 (6)

where ∂_J includes all possible partial derivatives and J denotes any of the jet space variables being used. (For example, in the harmonic oscillator and pendulum examples,

⁴The notation here is as usual: $u_x = \partial u/\partial x$, $u_{xx} = \partial^2 u/\partial x^2$, etc.

 $J=\{u,\dot{u}\}$; for the Duffing oscillator $J=\{t,u,\dot{u}\}$. However, the time derivative would only be applied to variables with an explicit time dependence, such as p(t), but not u or \dot{u} .) If there are any special symmetry considerations, that should also be included. This rubric is motivated by the expansion that results from the Runge-Kutta algorithm, and will be illustrated in the examples and in Appendix A. Finally, one should keep in mind that this rubric produces a *superset* of the terms that would result from a Runge-Kutta expansion. The extent to which every possible combination actually appears depends on the amount of nonlinearity in the underlying DE. In particular, linear problems like the harmonic oscillator have no contributions beyond the first derivative.

For example, in the case of the damped pendulum or damped harmonic oscillator, which obey a 2nd-order ODE and have no explicit time dependence, the surface \mathcal{D} in the space $\mathcal{J}^{(2)}=\{t,u,u^{(1)},u^{(2)}\}$ could describe the equation (and t will not be needed). Also, the response variables (Y) will be composed of updates (i.e., the Δ s) of $U^{(1)}=\{u,u^{(1)}\}$; note the highest order derivative isn't used. The choice of the set of predictor variables (X) is a bit more nuanced, and is often an iterative process. The modeler might begin with $\mathcal{J}^{(1)}$, realize only $U^{(1)}$ is needed (since there is no explicit time dependence), and then augment it using domain expertise. For example, for the pendulum the modeler might realize that since u is periodic, a better initial choice would be 5 $\mathcal{F}=\{\cos u,\sin u,\dot{u}\}$. This variable \mathcal{F} will fit into the left-hand side of Eq. 6, and the right-hand side would produce additional suggested terms to use for predictors (cf. Eq. 32b).

Finally, modeling in this paper will attempt to place additional complexity into the initial input features, thereby lessening the need for complexity in the remaining part of the model. It is claimed here that this may be a general principle, that the sum of the complexity of the initial features and the complexity of the remaining part of the model is roughly constant; this would be true across different models with similar performance.

2.5 Constants of Motion

The general approach of this paper has been to model Δu and $\Delta \dot{u}$ for small time steps. As the intent will be to apply this modeling procedure to physical problems, where symmetries (such as conservation of energy, momentum, etc) are present, it begs the question of whether it would be fruitful to study the problem from the vantage point of Lie symmetries applied to DEs, as they take a similar tack. For that reason, this section will study several points of Lie symmetries, which will be applied to each of the three examples to follow.

As discussed in Sec. 2.1, a solution to an ODE can be understood as being a curve in the surface $\mathcal{D}=0$. If a diffeomorphism (here, a point transformation) of the underlying variables, defined as

$$t \to \tilde{t}(t, u; \epsilon)$$
$$u \to \tilde{u}(t, u; \epsilon)$$

 $^{^5}$ The variable name $\mathcal F$ is used generically for a set of features. In the examples it will become synonymous with the variable X.

subject to the constraints

$$\tilde{u}^{(k)} = \frac{d^k \tilde{u}}{d\tilde{t}^k}, \quad k = 1, \dots, n$$

and the initial conditions $\tilde{t}(t, u; 0) = t$ and $\tilde{u}(t, u; 0) = u$ is such that

$$\mathcal{D}(\tilde{t}, \tilde{u}, \tilde{u}^{(1)}, ..., \tilde{u}^{(n)}) = 0$$

then it is called a Lie symmetry of the ODE.

Defining the rates of change of these transformed coordinates as

$$\xi = \frac{d\tilde{t}}{d\epsilon}\Big|_{\epsilon=0}, \quad \eta = \frac{d\tilde{u}}{d\epsilon}\Big|_{\epsilon=0}, \quad \eta^{(k)} = \frac{d\tilde{u}^{(k)}}{d\epsilon}\Big|_{\epsilon=0}$$

allows the transformed coordinates to be written as

$$\tilde{t} = t + \epsilon \xi + \mathcal{O}(\epsilon^2)$$

$$\tilde{u} = u + \epsilon \eta + \mathcal{O}(\epsilon^2)$$

$$\tilde{u}^{(k)} = u^{(k)} + \epsilon \eta^{(k)} + \mathcal{O}(\epsilon^2)$$

where $\eta^{(k)}$ is the kth prolongation of η (it is not the kth derivative).

When Lie symmetries are studied in DEs it is normally for the purpose of identifying symmetries that can be used to parametrize families of solutions, and so solve the equation from that vantage point. In this paper however, the symmetry arises from a simple evolution of the system forward in time. So in this case the first few equations are

$$\tilde{t} = t + \epsilon \tag{7}$$

$$\tilde{u} = u + \Delta u \tag{8}$$

$$\tilde{u}^{(1)} = u^{(1)} + \Delta u^{(1)} \tag{9}$$

where Δu , $\Delta u^{(1)}$ are understood in the sense of Sec. 2.2, and $\dot{u} \equiv u^{(1)}$. The plan then is to use other Lie symmetry techniques in the study of the dynamics as $\epsilon \to 0$.

A Lie symmetry of this DE can also be understood as defining a flow (\mathcal{X}) on the jet space [Olver, 1993, Bluman and Kumei, 1989, Hydon, 2000]

$$\mathcal{X} = \xi \frac{\partial}{\partial t} + \eta \frac{\partial}{\partial u} + \eta^{(1)} \frac{\partial}{\partial u^{(1)}} + \dots$$
 (10)

where the Lie symmetry is expressed as $\mathcal{X}\mathcal{D}=0$. An invariant \mathcal{I} of this symmetry will satisfy $\mathcal{X}\mathcal{I}=0$, and can be solved for using the method of characteristics

$$\frac{dt}{\varepsilon} = \frac{du}{n} = \frac{du^{(1)}}{n^{(1)}} + \cdots \tag{11}$$

For example, using the equation with du and $du^{(1)}$, an invariant would appear as a constant of integration (r) from the indefinite integrals

$$r = -\int^{u} \frac{du}{\eta} + \int^{u^{(1)}} \frac{du^{(1)}}{\eta^{(1)}}$$
 (12)

which might instead have been solved for as

$$r = -\int_{-}^{u} du \, \eta^{(1)} + \int_{-}^{u^{(1)}} du^{(1)} \, \eta \tag{13}$$

Also, since a function of a constant is still a constant, various transformations of r may be made for convenience; this will be done in the first example.

However, in the more numerical setting of an ML application where analytical expressions for η and $\eta^{(1)}$ are unavailable, a different approach is needed. In that case, one might instead compute the change in r as δr , computed as a *definite* integral along the trajectory Γ

$$\delta r = -\int_{\Gamma} du \, \eta^{(1)} + \int_{\Gamma} du^{(1)} \, \eta \tag{14}$$

In this approach, δr is zero (by definition), and thus what one hopes to gain is an understanding of the various contributions to it.

3 Example: Harmonic Oscillator (damped)

The equation for a harmonic oscillator is relevant for a myriad of physical systems, such as the small angle limit of a pendulum. Here, u represents the deviation from the minimum, and ω_0 its natural frequency

$$\ddot{u} + 2\gamma \dot{u} + \omega_0^2 u = 0. \tag{15}$$

Its general solution in the underdamped case is $u = Ae^{-\gamma t}\cos(\omega t + \alpha)$, where $\omega = \sqrt{\omega_0^2 - \gamma^2}$, A is the amplitude, and α is the phase. This section will mostly consider the case of $\gamma \neq 0$, except where stated otherwise.

Training Data

For the present example, training data was generated from 2000 random samples 6 , using $\omega_0=1, \gamma=0.1, t\in(0,2T), u\in(-2,2), \dot{u}\in(-2,2)$. Data point pairs were created using a randomly sampled point, with a new point being created via a single step of a 4th-order Runge-Kutta scheme; the time step was $\epsilon=0.1$. In the center and right plots in Fig. 3, only the first of each pair is plotted, since the points are so close to each other; the left plot was created from a single trajectory. In the center and right plots, the

⁶Far fewer were needed to get a good fit. This number of points was chosen in order to create a clear visual for Δu and $\Delta \dot{u}$.

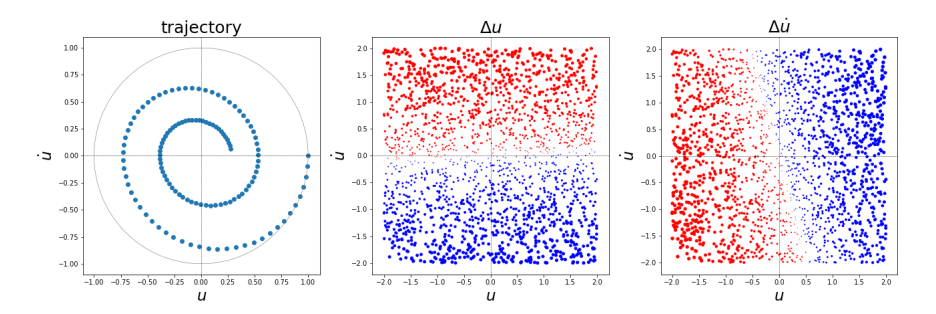


Figure 3: The left plot corresponds to the (clockwise) path taken by updates of the system, starting from an initial condition of $(u, \dot{u}) = (1, 0)$. The light gray circle is added as a visual reference, and corresponds to the path that would have been taken in the undamped case. The center and right plots correspond to the changes in u and \dot{u} , as defined in Eq. 3. The dot sizes are proportional to the magnitude of what is being plotted, and is red (blue) for positive (negative) values.

color of the points is determined by the sign of Δu or $\Delta \dot{u}$: it is red (blue) if the sign is positive (negative). Also, the size of the dots are proportional to the magnitude of Δu (or $\Delta \dot{u}$); the same scaling was used for both plots in the figure. These figures provide useful information as to how to model Δu and $\Delta \dot{u}$ over this space. Importantly, it appears that there are no "high variance" regions. Such regions would have, for example, a co-location of red and blue dots, or dots of markedly different sizes. Either of those could be detected numerically by measuring the variance (of Δu or $\Delta \dot{u}$) as a function of (u,\dot{u}) .

Model

Given these observations, it appears that it would suffice from a modeling perspective to simply have h_1 and h_2 be linear combinations of u and \dot{u} . However, following the guidance from Eq. 6, a large class of potential features ⁷ are considered.

$$\{u, \dot{u}\} \to \{u, \dot{u}, t, t^2, u^2, u\dot{u}, \dots\}$$

It will be understood from Appendix A that several of these terms need not be considered (such as t, t^2) for dynamics with no explicit time dependence.

As already discussed, while many ML models can be used (such as a NN), it is convenient here to use *feature regression*, since it will facilitate determining the underlying DE. After following the usual steps in regression ⁸, the resulting response

 $^{^{7}}$ Expect no constant term, since it appears the dot size is zero near the origin, in both plots in Fig. 3. Also, note that if \ddot{u} were included in the predictors, a collinearity would manifest itself, a signal to the developer that it should be removed.

⁸The only variables now considered are those that made a significant contribution.

(Y) and predictor (X) variables are chosen to be

$$Y = (\Delta u, \Delta \dot{u})^T \tag{16}$$

$$X = (u, \dot{u})^T \tag{17}$$

and the feature regression model h(X) appears as a matrix-vector product,

$$Y = \epsilon \begin{bmatrix} a_1 & a_2 \\ b_1 & b_2 \end{bmatrix} X \tag{18}$$

In this approach, one can now determine the coefficients a_i and b_i (i=1,2) using only regression. Using the time step $\epsilon=0.1$, the resulting values for these coefficients are shown in the center column in Table 1. In the feature regression modeling, regularization

	$\epsilon = 0.1$	$\epsilon \to 0$
$\overline{a_1}$	-0.050	0
a_2	0.988	1
b_1	-0.988	-1
b_2	-0.247	-0.2

Table 1: In the center column are values of the coefficients when $\epsilon=0.1$. The right column contains those same values after extrapolating to $\epsilon\to 0$, and are derived in the next section.

was not used, in contrast to approaches by other authors [eg. Crutchfield and McNamara, 1987, Rudy et al., 2017]. In that case, one might have used for example elastic net regularization [Hastie et al., 2009] to drive small, less important coefficients down to zero, enabling an easier identification of a "minimal model". Instead, in this paper the ϵ -dependence of these parameters will be studied, to determine their behavior as $\epsilon \to 0$ and ascertain the underlying DE.

Underlying DE

Next, the values for these coefficients are found in the limiting case of $\epsilon \to 0$. Graphs for the behavior of these coefficients are shown in Fig. 4. The data was based on fitting these coefficients with a mapping using values for ϵ from 0.1 to 0.001. Upon extrapolating a polynomial fit of these plots to $\epsilon=0$, the values in the rightmost column of Table 3 resulted. Deviations in these values due to the fit were on the order of 10^{-15} to 10^{-17} . The mapping of Eq. 18 may now be rewritten in this limiting case, and the variables will be written using the standard differential notation (ie, $\epsilon \to dt$, $\Delta u \to du$, $\Delta \dot{u} \to d\dot{u}$), producing

$$du = dt[\dot{u}] \tag{19a}$$

$$d\dot{u} = dt[-0.2\dot{u} - u] \tag{19b}$$

The first of these equations (Eq. 19a) is just a contact condition, and reflects the fact that in the space (u, \dot{u}) , not all three quantities du, dt, \dot{u} are independent (i.e., $\dot{u} = du/dt$)

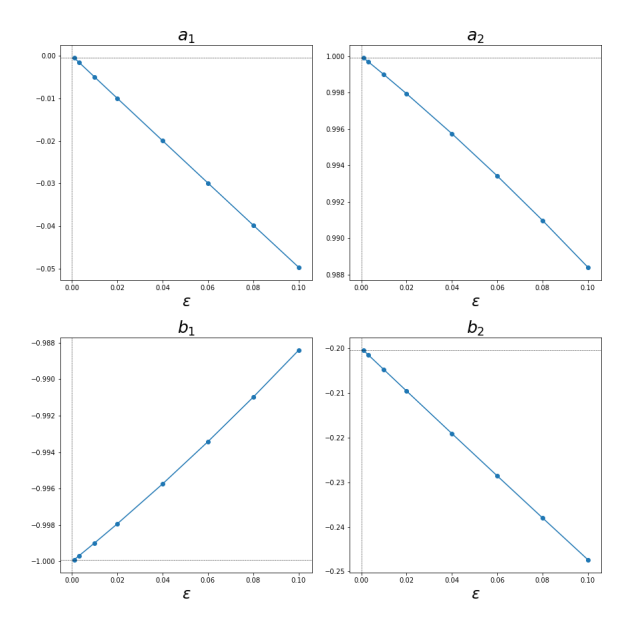


Figure 4: Plots of the ϵ -dependence of the a_i coefficients (i=1,2) in the model h(X) (cf. Eq. 18). The values obtained by extrapolating these curves to $\epsilon=0$ are listed in Table 1.

⁹ . The second of these equations (Eq. 19b) is just equivalent to the original equation of motion for the pendulum (Eq. 15), with the chosen parameter values ($\omega_0=1$ and $\gamma=0.1$).

3.1 Parameter Dependence

What was obtained in the previous section is the equation of motion based on the choice $\omega_0=1,\,\gamma=0.1$. In this section, the actual functional dependence on ω_0 and γ within the equation of motion is deduced.

The idea here is to consider a given value of ϵ , and several values of ω_0 . This produces a plot versus ω_0 , which is then fit with a low-order polynomial in ω_0 . Thus, the fitting parameters are now determined for that one, given value of ϵ . Next, this procedure is repeated for several other small values of ϵ , and the result is extrapolated to $\epsilon=0$. The results differed from the expected exact values only on the order of machine precision (about 10^{-15}).

$$b_1 = -\omega_0^2 + \dots (20)$$

$$b_2 = -2\gamma + \dots (21)$$

Shown in Fig. 5 is the ω_0 and γ dependence for these parameters in the specific case of $\epsilon = 0.001$. From this, now know that Eq. 19a and Eq. 19b can be replaced with

⁹Of course, this is a slight abuse of notation, since derivatives are normally defined in a limiting procedure.

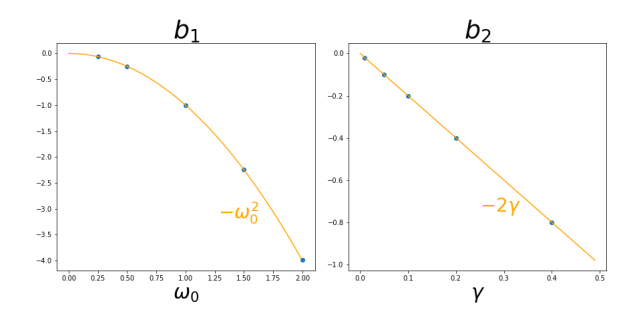


Figure 5: Comments... as a visual guide, the exact curves for $-\omega_0^2$ and -2γ are added to the left and right plots, respectively.

$$du = dt[\dot{u}] \tag{22}$$

$$d\dot{u} = dt[-\omega_0^2 u - 2\gamma \dot{u}] \tag{23}$$

from which the original equation of motion (Eq. 15) immediately follows. In summary, it has been shown how to obtain the complete equation of motion (along with parameter dependence), from data.

Extrapolation & Stability

The ability of this model to extrapolate beyond the original training data can also be demonstrated. Using the model parameter values found using $\epsilon=0.1$ (i.e, the center column in Table 1), and following the rubric of the generative algorithm, Fig. 6 results.

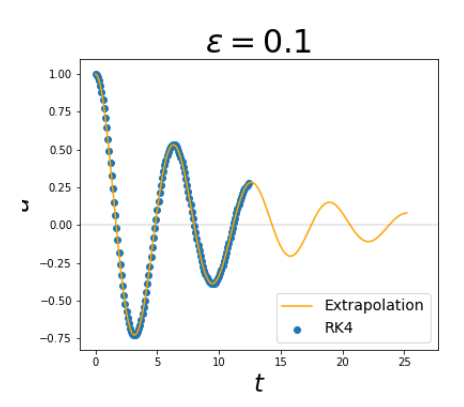


Figure 6: A comparison of the extrapolation of FJet to data generated by RK2, over the time range used for the training data (0, 2T), where $T = 2\pi/\omega_0$.

The stability is assessed in the case $\omega_0 = 1$, $\gamma = 0$, so that it can easily be compared to a known theoretical solution for the decay of the energy [Young, 2020], which is

expressed as

$$E_n/E_0 = \exp(\lambda n) \tag{24}$$

at the *n*th iteration. Thus, a λ closer to 0 means it is more stable. Computing E_n for all cases and determining λ from that led to the values in Table 2. The most obvious

scheme	λ
Euler	9.94×10^{-2}
RK2	2.49×10^{-5}
RK4	-1.38×10^{-8}
FJet	-1.63×10^{-17}

Table 2: Note that (in the undamped case) FJet remains stable about 10^9 times longer than RK4 in this example. A simulation was run for 10,000 iterations, with the initial condition of $(u, \dot{u}) = (1, 0)$. These results were computed for the $\gamma = 0$ case.

aspect to this table is that λ is about 10^9 times smaller than the λ for RK4, which means it remains stable for about 10^9 times longer compared to RK4. These values agree extremely well with an analytical solution in Appendix C.

3.2 Constants of Motion

It has been shown how to model the data for Δu and $\Delta \dot{u}$, and to determine the parameter dependencies in the small- ϵ limit, which yields

By considering these updates through the lens of Lie symmetries of a DE, one can identify that for a translation in the independent variable (time) by the amount ϵ there is an associated rate of change in u and \dot{u} with

$$\eta = h_1/\epsilon \tag{26}$$

$$\eta^{(1)} = h_2/\epsilon \tag{27}$$

The next step will be to use these expressions in connection with Eq. 14 to understand how the various terms in h_1 and h_2 contribute along a trajectory $\Gamma(t)$ from $(u(0), \dot{u}(0))$ to $(u(t), \dot{u}(t))$.

$$\delta r(t) = -\int_{\Gamma} du \, \eta^{(1)} + \int_{\Gamma} d\dot{u} \, \eta \tag{28}$$

$$= \delta E + w_{diss} \tag{29}$$

where

$$\delta E = \omega_0^2 \int_{\Gamma} du \, u + \int_{\Gamma} d\dot{u} \, \dot{u} \tag{30a}$$

$$w_{diss} = 2\gamma \int_{\Gamma} du \, \dot{u} \tag{30b}$$

Eq. 30a is the change in energy from the initial condition, and Eq. 30b is the work done by dissipative forces (i.e., just the force $(2\gamma u)$ integrated over the distance u). Their sum, δr , is zero, and the three are plotted in Fig. 7 What is noticeable is that

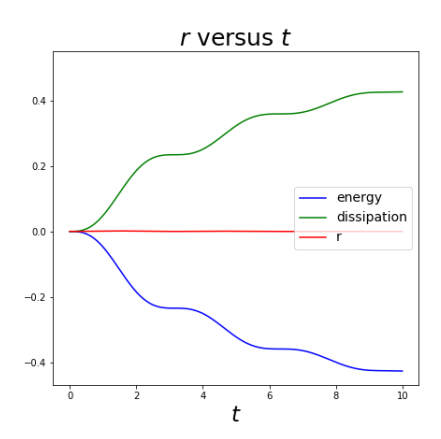


Figure 7: Using the initial conditions $(u, \dot{u}) = (1, 0)$, and computing the change in energy and energy lost to dissipation along a trajectory as a function of time in the damped case $(\gamma = 0.1)$. Note that the sum of these contributions (δr) is constant.

 δr remains at 0, as it should, and the loss in the energy equals the work done by the dissipation. In contrast, in a physics context the only constants of motion normally found are conserved quantities, such as the energy or momentum, for example. In this case, the conserved quantity r corresponds to the energy (or a function thereof) of the larger system (including u(t) and the dissipation). It could also be interpreted as the initial energy plus δr in this case. Next, the constant r will be computed for all values in the (u,\dot{u}) plane.

Phase Space ($\gamma = 0$)

The case where there is no dissipation (i.e., $\gamma=0$) is straightforward and r is easily found (using Eqn. 14, for example)

$$r(u, \dot{u}) = \frac{1}{2} \left[\omega_0^2 u^2 + \dot{u}^2 \right]$$

If this represents a physical system of a mass (m) on a spring (with constant k), then the energy is mr. Contour plots for this function are not shown, since they are just ellipses.

Phase Space ($\gamma \neq 0$)

The case where there is dissipation (i.e., $\gamma \neq 0$) leads to qualitative changes in $r(u, \dot{u})$. The details of the calculation are in Appendix C, and lead to

$$r_n(u, \dot{u}) = \frac{1}{2} [\omega^2 u^2 + (\gamma u + \dot{u})^2] \exp\left(2\frac{\gamma}{\omega}\phi_n\right)$$

where

$$\tan \phi = -(\gamma u + \dot{u})/(\omega u)$$
$$\phi_n = \phi + 2n\pi$$

and n=...,-2,-1,0,1,2,... This expression for the contours is unique in that it now depends on Riemannian sheets, with n=0 indicating the principal sheet. The angle ϕ is computed so that its range is $[0,2\pi)$ and increases in a clockwise manner; it is measured from the branch cut (where $\dot{u}=-\gamma u$).

In Fig. 8 this constant is plotted for the sheets n=0 and n=1 The dissipation

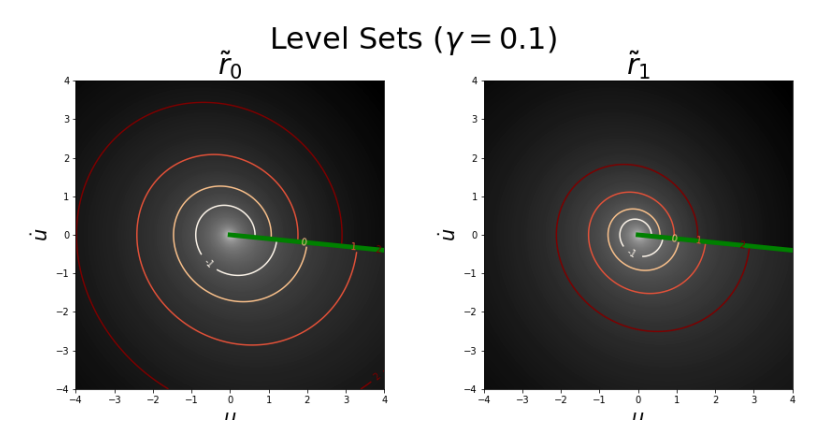


Figure 8: Contour plots for the harmonic oscillator showing where r_n is constant; this was plotted in terms of $\tilde{r}_n = \log(2r_n)$ for ease in graphing. The green line indicates a branch cut in the contour surface. The dynamics of the system lead to a clockwise rotation, staying on such a contour.

causes the curves to spiral inward in a clockwise fashion. The branch cut (the green line) limits the beginning and end of a trajectory. Thus when a trajectory reaches a branch cut, it jumps to the next highest sheet. The differently colored curves in each plot each have their own value; they act as level sets for this contour plot. As can be seen, the value of r is continuous except in the neighborhood of the branch cut. When crossing the branch cut from above (below) the branch cut, the sheet number increases (decreases). Note that these curves replace the energy contours used to characterize an undamped oscillator.

4 Example: Pendulum (damped)

The damped pendulum is an important extension of the harmonic oscillator from the last example, in that it introduces nonlinearities and periodicity. The equation of motion is

$$\ddot{u} + 2\gamma \dot{u} + \omega_0^2 \sin u = 0 \tag{31}$$

where ω_0 is the natural frequency in the small-u limit and γ is the damping coefficient.

Training Data

The parameter values $\omega_0=1.0$ and $\gamma=0.1$ are used in Fig. 9, which includes multistart trajectories (left plot), and update maps for Δu and $\Delta \dot{u}$ (center and right plots). Note that in the left plot, the rotation is clockwise; in the upper (lower) half of the

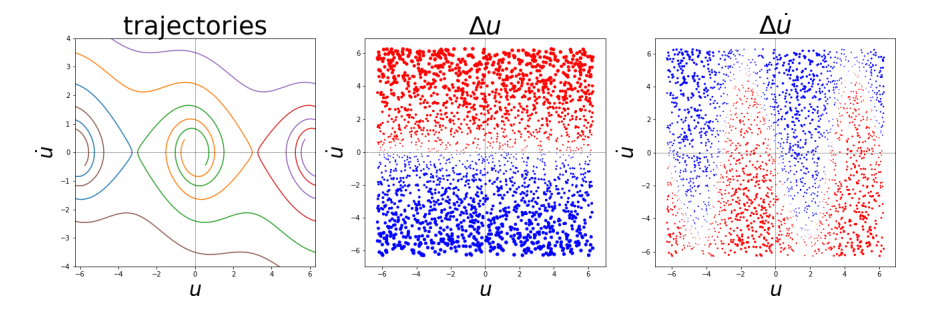


Figure 9: The left plot corresponds to the paths taken by updates of the system, starting from a number of different initial points. Note the 2π periodicity along u. The center and right plots correspond to the changes in u and \dot{u} , as defined in Eq. 3. The dot sizes are proportional to the magnitude of what is being plotted, and is red (blue) for positive (negative) values.

plane, the motion is to the right (left). As discussed before, the Δ plots were created by randomly selecting (u,\dot{u}) values and then doing a single time step update (with $\epsilon=0.1$), in this case using RK2. This created a data pair, and allowed a creation of Δu and $\Delta \dot{u}$; the red (blue) colors indicate positive (negative) values. It is these plots which will be fitted by an ML procedure, such as NNs, feature regression, random forest regressors, etc [Hastie et al., 2009]. Also, the three plots in this figure have u and \dot{u} each range over $(-2\pi, 2\pi)$ to display the periodic structure, but in the actual training data only the range of $(-\pi, \pi)$ was used.

Model

As a starting assumption, based on experience with a harmonic oscillator (cf. Sec. 3), one might begin by considering the feature set $\{u,\dot{u}\}$. However, the domain knowledge in this case is that u must be periodic, so instead the starting feature set under consideration is $\{\dot{u},\cos u,\sin u\}$. As discussed in Sec. 2.4, numerical integration techniques (cf. Appendix A) suggest one should use a larger feature set, such as

$$\{\dot{u}, \cos u, \sin u\} \rightarrow \{\dot{u}, \cos u, \sin u, \dot{u} \cos u, \dot{u} \sin u, \dots\}$$

The elements in this new set may now be taken as input features into an appropriate ML model. As already discussed, while many ML models can be used (such as NNs), it is convenient here to use *feature regression*, since it will facilitate determining the underlying DE. After following the usual steps in regression, the resulting response (Y)

and predictor (X) variables are chosen to be

$$Y = (\Delta u, \Delta \dot{u})^T \tag{32a}$$

$$X = (\dot{u}, \sin u, \dot{u}\cos u)^T \tag{32b}$$

and the feature regression model h(X) appears as a matrix-vector product,

$$Y = \epsilon \begin{bmatrix} a_1 & a_2 & a_3 \\ b_1 & b_2 & b_3 \end{bmatrix} X \tag{33}$$

In this approach, one can now determine the coefficients a_i and b_i (i=1,2,3) using only polynomial regression in ϵ . Using the time step $\epsilon=0.1$, the resulting values for these coefficients are shown in the center column in Table 3. In the feature regression

	$\epsilon = 0.1$	$\epsilon \to 0$
$\overline{a_1}$	0.990	1
a_2	-0.049	0
a_3	0	0
b_1	-0.197	-0.2
b_2	-0.985	-1
b_3	-0.049	0

Table 3: In the center column are values of the coefficients when $\epsilon = 0.1$. The right column contains those same values after extrapolating to $\epsilon \to 0$, and are derived in the next section.

modeling, regularization was not used, in contrast to approaches by other authors [eg. Crutchfield and McNamara, 1987, Rudy et al., 2017].

Underlying DE

Next, the values for these coefficients are found in the limiting case of $\epsilon \to 0$, using the same approach as in the previous examples. Graphs for the behavior of these coefficients are shown in Figs. 10, 11. The data was based on fitting these coefficients with a

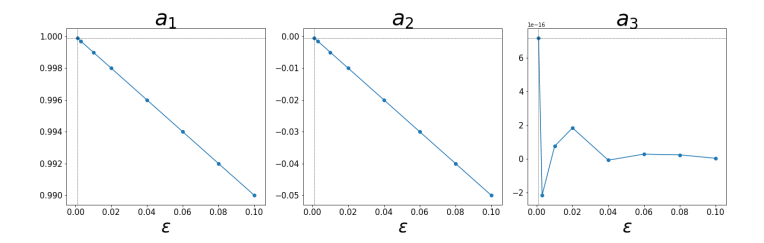


Figure 10: Plots of the ϵ -dependence of the a_i coefficients (i = 1, 2, 3) in the model h(X) (cf. Eq. 33).

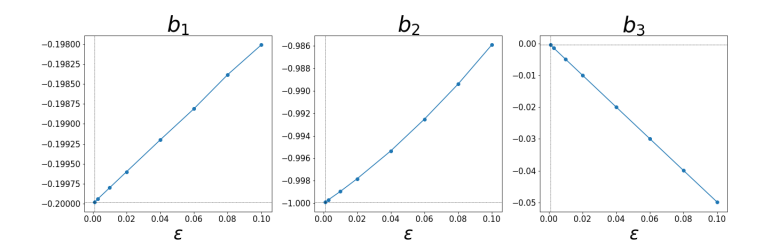


Figure 11: Plots of the ϵ -dependence of the b_i coefficients (i=1,2,3) in the model h(X) (cf. Eq. 33).

mapping using values for ϵ from 0.1 to 0.001. Upon extrapolating a polynomial fit of these plots to $\epsilon=0$, the values in the rightmost column of Table 3 resulted. The mapping of Eq. 33 may now be rewritten in this limiting case, and the variables will be written using the standard differential notation (ie, $\epsilon \to dt$, $\Delta u \to du$, $\Delta \dot{u} \to d\dot{u}$), producing

$$du = dt[\dot{u}] \tag{34a}$$

$$d\dot{u} = dt[-0.2\dot{u} - \sin u] \tag{34b}$$

The first of these equations (Eq. 34a) is just a contact condition, and reflects the fact that in the space (u,\dot{u}) , not all three quantities du,dt,\dot{u} are independent (i.e., $\dot{u}=du/dt$) ¹⁰. The second of these equations (Eq. 34b) is just equivalent to the original equation of motion for the pendulum (Eq. 31), with the chosen parameter values.

Extrapolation & Stability

The ability of this model to extrapolate beyond the original training data can also be demonstrated. Using the model parameter values found in the undamped case ($\gamma=0$), using $\epsilon=0.1$ (i.e, the center column in Table 3), and following the rubric of the generative algorithm (Algo. 1), Fig. 12 results. In addition, the stability can be assessed by a long time comparison between the extrapolation of FJet and RK2. In Fig. 13, is shown the energy (left plot), the absolute value of the difference ¹¹ between the solutions (center plot), and an examination at late times of the phase difference between the two (right plot). The energy is computed as

$$E = \frac{1}{2}\dot{u}^2 + \omega_0^2 (1 - \cos u) \tag{35}$$

and is shown as a faint gray line in the left plot. Since the initial condition is $(u, \dot{u}) = (1, 0)$, the energy is $1 - \cos(1) \approx 0.46$.

¹⁰Of course, this is a slight abuse of notation, since derivatives are defined in a limiting procedure.

¹¹A technique for reducing the errors in the center plot will be presented in a later version of this preprint.

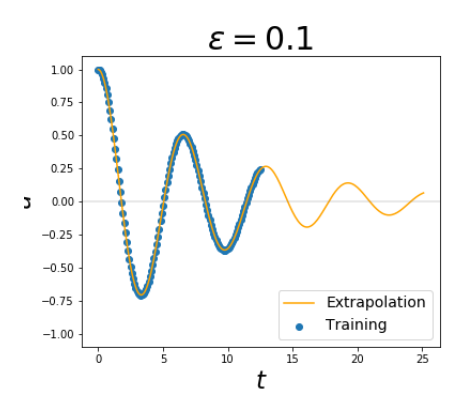


Figure 12: A comparison of the extrapolation of FJet to data generated by RK2 in the damped case ($\gamma = 0.1$), over the time range used for the training data (0, 2T), where $T = 2\pi/\omega_0$.

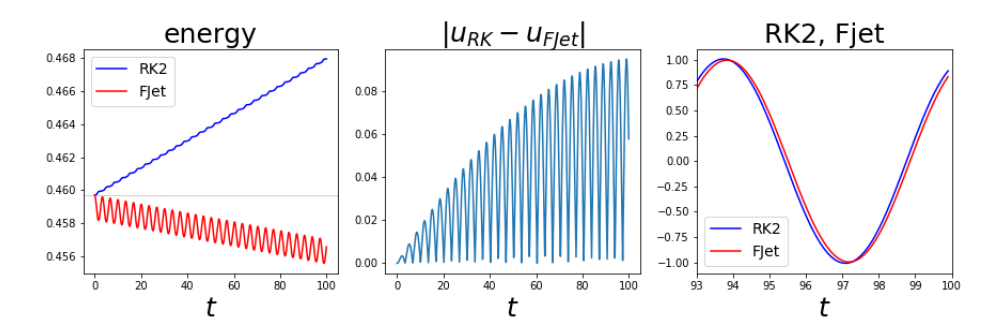


Figure 13: Three plots indicating the difference between the extrapolation from FJet and RK2 in the undamped case ($\gamma=0$). The left plot compares the energy for each, using Eq. 35. The center plot is of the absolute value of the difference between the two solutions, plotted as a function of time. The right plot compares the two solutions, after about 15 periods.

Constants of Motion

Again interpreting h_1/ϵ as η , and h_2/ϵ as $\eta^{(1)}$ in the $\epsilon\to 0$ limit of the feature regression model, it follows

$$\begin{bmatrix} \eta \\ \eta^{(1)} \end{bmatrix} = \begin{bmatrix} 0 & 1 \\ -\omega_0^2 & -2\gamma \end{bmatrix} \begin{bmatrix} \sin u \\ \dot{u} \end{bmatrix}$$
 (36)

Following Sec. 2.5, the constant of motion from integration results in

$$\delta r(t) = -\int_{\Gamma} du \, \eta^{(1)} + \int_{\Gamma} d\dot{u} \, \eta \tag{37}$$

$$= \delta E + w_{diss} \tag{38}$$

where

$$\delta E = \omega_0^2 \int_{\Gamma} du \sin u + \int_{\Gamma} d\dot{u} \,\dot{u} \tag{39}$$

$$w_{diss} = 2\gamma \int_{\Gamma} du \,\dot{u} \tag{40}$$

are computed along the trajectory $\Gamma(t)$ from $(u(0),\dot{u}(0))$ to $(u(t),\dot{u}(t))$. Here, δE is the change in energy, and w_{diss} is the energy lost through dissipation (i.e., because of the damping force). Integrating these quantities along a path in phase space (with initial condition $((u,\dot{u})=(1,0))$ yields Fig. 14. Once again, it is shown that δr is a

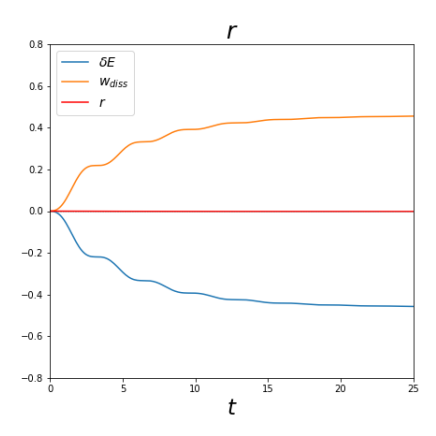


Figure 14: Using the initial conditions $(u, \dot{u}) = (1, 0)$, and computing the change in energy and energy lost to dissipation along a trajectory as a function of time in the damped case $(\gamma = 0.1)$. Note that the sum of these contributions (δr) is constant.

constant. Also, δr may again be interpreted as the change of the energy of the system and environment, which is zero; it is expressed here, since $\delta r=0$, as $\delta E=-w_{diss}$. However, the reader is cautioned that this is not a general feature of this Lie symmetry technique, which doesn't require a physical context. Finally, note that if $\gamma=0$, the integration could easily be done, reproducing the expression for the energy given in Eq. 35.

5 Example: Duffing Oscillator

The Duffing oscillator [Duffing, 1918, Moon and Holmes, 1979, Jackson, 1991] is based on the damped oscillator seen in Sec. 3, except it is augmented by a nonlinear restoring term (proportional to β), a force p(t), and α is allowed to be negative. It appears here as

$$\ddot{u} + 2\gamma \dot{u} + \alpha u + \beta u^3 = p(t) \tag{41a}$$

$$p(t) = A\sin\Omega t \tag{41b}$$

Training Data

Throughout this example, unless specified otherwise, the parameter values will be: $\gamma=0.15, \, \alpha=-1, \, \beta=1, \, A=0.28, \, {\rm and} \, \Omega=1.2.$ These values are used to create Fig. 15. The left plot was created from a single run with initial condition $(u,\dot{u})=(1,0)$;

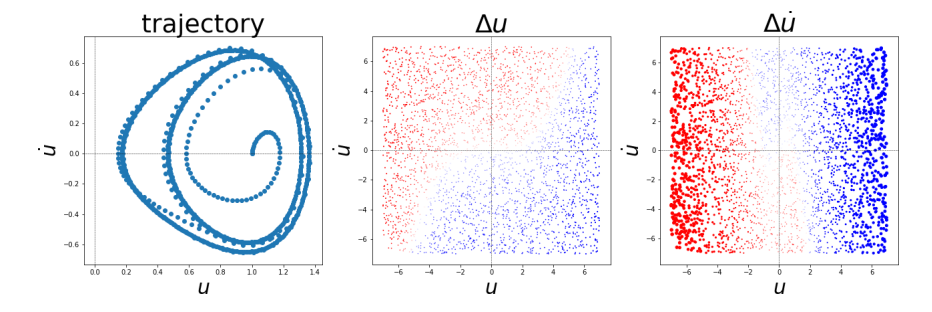


Figure 15: The left plot corresponds to the paths taken by updates of the system, starting from a number of different initial points. Note that the orbit is in the period-2 phase. The center and right plots correspond to the changes in u and \dot{u} , as defined in Eq. 3. The dot sizes are proportional to the magnitude of what is being plotted, and is red (blue) for positive (negative) values. Also, note the different scale of the left plot compared to the center and right plots.

the updates are in a clockwise rotation and reveal a period-2 oscillation. The center and right plots are update maps for Δu and $\Delta \dot{u}$. The first step in creating the training data was to randomly sample (u,\dot{u},t) ; the random time was inserted into Eq. 41b to create sampling for p and \dot{p} . The second step was to then do a single time step update with RK2 using $\epsilon=0.1$. This created a data pair, and allowed a creation of Δu and $\Delta \dot{u}$.

With a keen eye, the reader may note that in the right plot of Fig. 15 there is a slight overlap between positive (red) and negative (blue) dots. This results in a larger variance in the values and indicates that these two variables aren't sufficient to model Δu and $\Delta \dot{u}$ (i.e., the set of predictor variables needs to be augmented). Also, in anticipation of using p and \dot{p} as predictors, those data were also collected and stored for each Δu and $\Delta \dot{u}$.

Model

As a starting assumption, based on experience with a harmonic oscillator (cf. Sec. 3), one might begin by considering the feature set $\{u,\dot{u},p\}$. However, as discussed in Sec. 2.4, numerical integration techniques (cf. Appendix A) suggest one should at first consider using a larger feature set, such as

$$\{u, \dot{u}, p\} \rightarrow \{u, \dot{u}, u^2, u\dot{u}, \dot{u}^2, u^3, u^2\dot{u}, u\dot{u}^2, \dot{u}^3, p, \dot{p}, pu, p\dot{u}, \dot{p}u, \dot{p}\dot{u}, \dots\}$$

The elements in this new set may now be taken as input features into an appropriate ML model. As already discussed, while many ML models can be used (such as a NN), it is convenient here to use *feature regression*, since it will facilitate determining the

underlying DE. After following the usual steps in regression the resulting response (Y) and predictor (X) variables are chosen to be

$$Y = (\Delta u, \Delta \dot{u})^T \tag{42}$$

$$X = (u, \dot{u}, u^3, u^2 \dot{u}, u \dot{u}^2, \dot{u}^3, p, \dot{p})^T$$
(43)

and the feature regression model Y = h(X) appears as a matrix-vector product ¹²,

$$Y = \epsilon \begin{bmatrix} a_1 & a_2 & a_3 & 0 & 0 & 0 & a_7 & 0 \\ b_1 & b_2 & b_3 & b_4 & b_5 & b_6 & b_7 & b_8 \end{bmatrix} X$$
 (44)

In this approach, one can now determine the coefficients a_i and b_i (i=1,...,8) using only regression. Using the time step $\epsilon=0.1$, the resulting values for these coefficients are shown in the center column in Table 4. Note that the resulting FJet mapping can

	$\epsilon = 0.1$	$\epsilon \to 0$
$\overline{a_1}$	0.0500	0
a_2	0.9850	1
a_3	-0.0499	0
a_7	0.0499	0
b_1	0.9850	1
b_2	-0.2455	-0.3
b_3	-0.985	-1
b_4	-0.1499	0
b_5	-7.5×10^{-3}	0
b_6	-1.25×10^{-4}	0
b_7	0.9832	1
b_8	0.0499	0

Table 4: In the center column are values of the coefficients when $\epsilon = 0.1$. The right column contains those same values after extrapolating to $\epsilon \to 0$, and are derived in the next section. The coefficients a_4 , a_5 , a_6 , and a_8 are close to zero and so are disregarded.

then make use of any forcing term to be used in an extrapolation algorithm. Because of its reliance on a general p (and \dot{p}), it resembles a Green's function approach.

In the feature regression modeling, regularization was not used, in contrast to approaches by other authors [eg. Crutchfield and McNamara, 1987, Rudy et al., 2017]. For example, one might have used regularization to drive small, less important coefficients down to zero, enabling an easier identification of a "minimal model". Instead, the ϵ -dependence of these parameters will be studied, to determine their behavior as $\epsilon \to 0$ and ascertain the underlying DE. However, if one is not interested in this limit, it would make sense to use regularization.

 $^{^{12}}$ As it turned out, the terms $u\dot{u}^2$ and \dot{u}^3 are not part of the recommended X for RK2 (see Appendix A). In the matrix below they correspond to parameters b_5 and b_6 ; note that these two parameters are noticeably smaller than the others.

Underlying DE

Next, the values for these coefficients are found in the limiting case of $\epsilon \to 0$, using the same approach as in the previous examples. Graphs for the behavior of these coefficients are shown in Figs. 16, 17. The time steps used in creating these figures ranged from

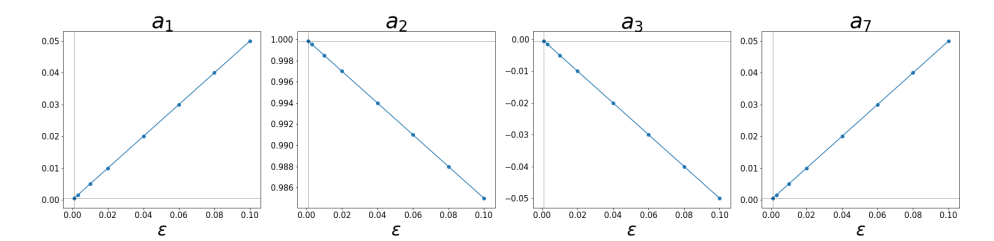


Figure 16: Plots of the ϵ -dependence of the a_i coefficients (i = 1, 2, 3, 7) in the FJet mapping matrix (cf. Eq. 44).

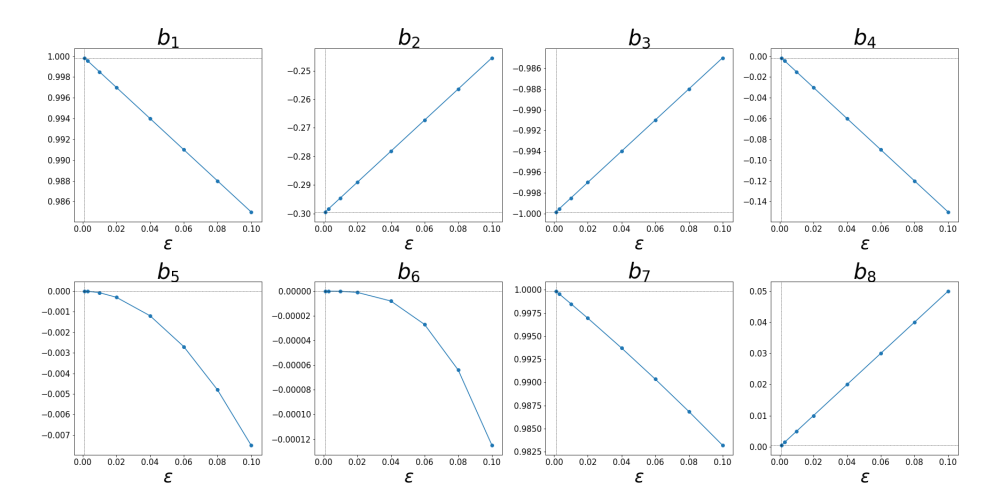


Figure 17: Plots of the ϵ -dependence of the b_i coefficients (i = 1, 2, ..., 8) in the FJet mapping matrix (cf. Eq. 44).

0.1 to 0.001. Upon extrapolating a polynomial fit of these plots to $\epsilon=0$, the values in the rightmost column of Table 4 resulted, and determined the underlying DE. With the standard differential notation (i.e., $\epsilon \to dt$, $\Delta u \to du$, $\Delta \dot{u} \to d\dot{u}$), the mapping produces

$$du = dt[\dot{u}] \tag{45a}$$

$$d\dot{u} = dt[u - 0.3\dot{u} - u^3 + p(t)] \tag{45b}$$

The first of these equations (Eq. 34a) is just a contact condition, and reflects the fact that in the space (u, \dot{u}) , not all three quantities du, dt, \dot{u} are independent (i.e., $\dot{u} = du/dt$)

¹³ . The second of these equations (Eq. 34b) is just equivalent to the original equation of motion for the Duffing oscillator (Eq. 41a), with the chosen parameter values.

Extrapolation & Stability

Extrapolations for u(t) will now be created; the FJet parameters used are in the center column of Table 4, where $\epsilon=0.1$. Recall that for this model the user has to have knowledge of the values of p and \dot{p} , both at training time and during the extrapolation. During training the values of p and \dot{p} are recorded, and are included in the feature set X for training. During extrapolation, new values for p and \dot{p} are fed into an extrapolation algorithm. To account for this difference, the generative algorithm (Algo. 1) is amended to Algo. 2. Because arbitrary values for p (and \dot{p}) can be fed into the algorithm during the

Algorithm 2: Generation step

```
Input: t_0, N, p(t), \dot{p}(t)

Init: t = t_0

Init: u = u(t)

Init: \dot{u} = \dot{u}(t)

for i = 0 to N do

p = p(t)

\dot{p} = \dot{p}(t)

tmp_1 h_1 = h_1(u, \dot{u}, p, \dot{p})

tmp_2 h_2 = h_2(u, \dot{u}, p, \dot{p})

u \leftarrow u + tmp_1 h_1

\dot{u} \leftarrow \dot{u} + tmp_2 h_2

t \leftarrow t + \epsilon

print(u, t)

end for
```

extrapolation, it is similar to the Green's function approach in that regard. In principle any smooth function can be used for p(t), but for the sake of numerical accuracy, it should be well approximated by its Taylor series expansion for small time steps.

As a first test, an extrapolation is created using the same p(t) used in training, producing Fig. 18. It illustrates the close match between FJet and the reference solution created with RK2 during an early time period (0 to 5T) as well as a later time period (95T to 100T), where T is the period of the driving force.

As a second test, a range of different p(t) were used during the generative process. They are parameterized by $p(t) = A' \cos \Omega t$, where Ω is the same as before, but now A' ranges over 0.1 to 0.6; recall that FJet was trained using A=0.28. A comparison was made between RK2 and FJet, and the difference between the two results is computed in the function

$$E_n = \max_{t \in (0, nT)} |u_{RK2}(t) - u_{FJet}(t)| \tag{46}$$

¹³Of course, this is a slight abuse of notation, since derivatives are defined in a limiting procedure.

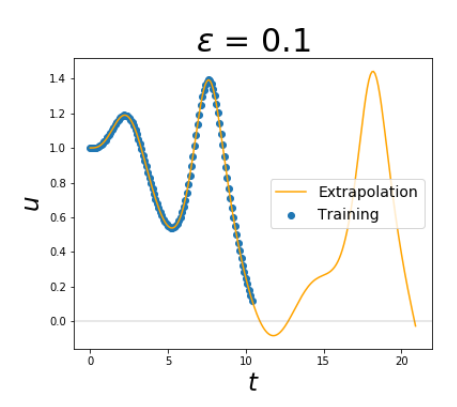


Figure 18: A comparison of the FJet extrapolation to RK2 over the time ranges (0, 5T) and (95T, 100T), where $T = 2\pi/\Omega$ is the period of p(t). Note the close similarity.

which measures the maximum absolute value of the difference, over the time range 0 to nT, where T is the period of p(t). Plots of $\log_{10} E_n$ are provided in Fig. 19 for n = 10, 20, 30, revealing that for times up through about 30T, Algo. 2 provides an

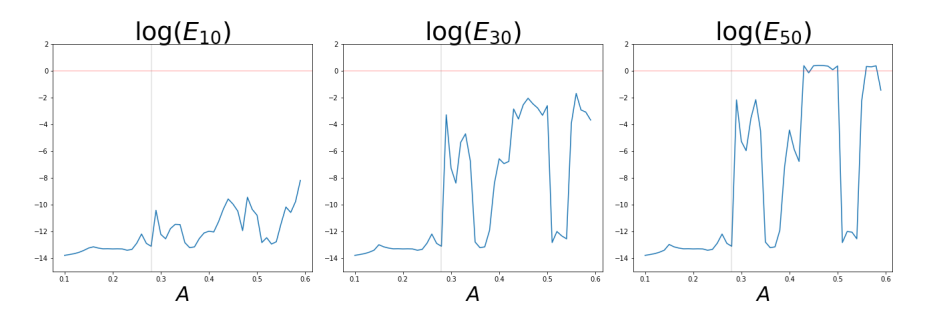


Figure 19: Three plots indicating a measure of the error between the extrapolation from FJet compared to the solution from RK2. The left, center and right plots correspond to $\log_{10} E_n$ (cf. Eq. 46) for n=10,30, and 50, where n is the number of periods of the driving force.

accurate approximation to RK2, even for values of A' that differ significantly from the value used for training (which is shown as a vertical gray line in the plots). Finally, comparisons were made to RK2, rather than RK4, since the complexity of the model (cf. Eq. 44) was at the level of RK2, as can be better understood after reviewing Appendix A.

Constants of Motion

Again interpreting h_1/ϵ as η , and h_2/ϵ as $\eta^{(1)}$ in the $\epsilon \to 0$ limit of the feature regression model, it follows

$$\begin{bmatrix} \eta \\ \eta^{(1)} \end{bmatrix} = \begin{bmatrix} 0 & 1 & 0 & 0 \\ -\alpha & -2\gamma & -\beta & 1 \end{bmatrix} \begin{bmatrix} u \\ \dot{u} \\ u^3 \\ p \end{bmatrix}$$
(47)

Following Sec. 2.5, the constant of motion from integration results in

$$\delta r(t) = -\int_{\Gamma} du \, \eta^{(1)} + \int_{\Gamma} d\dot{u} \, \eta \tag{48}$$

$$= \delta E - w_p + w_{diss} \tag{49}$$

where

$$\delta E = \int_{\Gamma} du \left(\alpha u + \beta u^3\right) + \int_{\Gamma} d\dot{u} \,\dot{u} \tag{50}$$

$$w_p = \int_{\Gamma} du \, p \tag{51}$$

$$w_{diss} = 2\gamma \int_{\Gamma} du \,\dot{u} \tag{52}$$

are computed along the trajectory $\Gamma(t)$ from $(u(0),\dot{u}(0))$ to $(u(t),\dot{u}(t))$, using the same parameter values from training (i.e., $A=0.28,\,\Omega=1.2,\,{\rm etc}$). Here, δE is the change in energy, w_p is the work done by the external force, and w_{diss} is the energy lost through dissipation (i.e., because of the damping force). Integrating these quantities along a path in phase space, with initial condition $(u,\dot{u})=(0,0)$, yields Fig. 20. Once again, it is shown that δr is a constant. Also, δr may again be interpreted as the change of the energy of the system and environment, which is zero; it is expressed here, since $\delta r=0$, as $\delta E=w_p-w_{diss}$. However, the reader is again cautioned that this is not a general feature of this Lie symmetry technique, which doesn't require a physical context.

6 Final Remarks

The FJet method has been introduced as an alternative means to model dynamical data, and in some cases the underlying DE and conserved quantities. It does so by performing ML modeling on updates in the phase space ¹⁴ of the system, rather than what competing methods use, a modeling over the time domain. In the FJet approach, the update data is formed by storing differences in the phase space variables over a small time step.

The FJet approach can be understood from the vantage point of the numerical integration scheme Runge-Kutta. By expanding an RK scheme with respect to the time step (ϵ) , certain features automatically appear. In the examples chosen, expansions of the RK2 scheme were done, and it was possible to know exactly what features should

 $^{^{14}}$ More generally it is $U^{(n-1)}$, when the underlying equation is of order n.

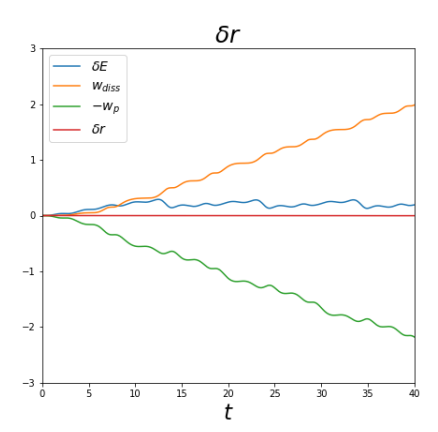


Figure 20: Using the initial conditions $(u, \dot{u}) = (0, 0)$, and computing the energy, dissipation, and power input along a trajectory as a function of time. Note that the sum of these contributions (δr) is constant. Also, note that δE seems to display a 2T-periodic behavior, consistent with this being in the period-2 phase.

be used in order to identify an equivalence to an RK scheme (RK2 or RK4, e.g.) at a given order of accuracy in ϵ . In the case where an external, time-dependent force was present, it was possible to understand what terms should be additionally included. The result was analogous to a Green's function approach (cf. Eq. 44 for Duffing oscillator). Finally, these considerations led to a general recommendation (Eq. 6) for what features to include, in the normal experimental scenario where the equation of motion isn't known beforehand.

While the modeling in this paper was done exclusively using feature regression, one should not make the mistake of thinking that it is a requirement. As pointed out at several points in the paper, any curve-fitting technique may be used. The reason for using feature regression is that it facilitates determining the underlying DE. If that is not a goal of the researcher, then other ML methods (such as NNs, XG-Boost, Random Forests) become competitive options.

In the three examples considered, it was demonstrated how the FJet model could lead to extrapolations beyond the range of the original training data. The accuracy of this extrapolation depends upon the number of variables, as well as the quality of the initial data for the updates (i.e., Δu , $\Delta \dot{u}$).

The initial features that are considered herein are relatively complex (e.g., $v \sin u$ in the Pendulum example) compared to other models, which commonly use a simple polynomial in u, for example. It is here asserted by the author that there is an interplay between the complexity of the initial features, and the complexity of the remaining ML model. In particular, it is asserted that for models of comparable (predictive) quality, the sum of these two complexities is constant. The author advocates for models with relatively complex initial features, as they make it easier to train and easier to understand the model, whether the remaining model be relatively simple (regression) or complex (NNs). Also, the initial features are a good place for the researcher to incorporate any

subject matter expertise (e.g., with respect to heuristics, constraints, symmetries, or physical laws).

Other researchers have similarly determined the underlying DE for a dynamical model. However, to the best of the author's understanding, they proceeded by performing a fitting for a small time step, while including a regularization term. In contrast, the approach taken here was not to use regularization, and instead perform several fits at different time steps, and then extrapolate the various coefficients to their value at vanishing time step (i.e., $\epsilon \to 0$). In doing this, excellent agreement was seen.

Acknowledgement

The author kindly acknowledges the insightful instruction on differential equations and dynamical systems from Prof. Julian I. Palmore and Prof. E. Atlee Jackson (d.) at U. Illinois at U.-C. during the author's undergraduate and graduate work there.

Appendix A: Runge-Kutta

The Runge-Kutta scheme [Press et al., 2007] is a standard technique for the numerical integration of a solution given its ODE. An *n*th-order explicit ODE can be rewritten as a system of first-order DEs, and thus the general form for the ODE can be expressed as

$$\frac{dy}{dt} = f(t, y) \tag{53}$$

where t(y) represents the independent (dependent) variables. The RK scheme involves an update from y_n to y_{n+1} , where the difference is

$$\Delta y_n \equiv y_{n+1} - y_n \tag{54}$$

After defining these quantities

$$k_1 = \epsilon f(t_n, y_n) \tag{55}$$

$$k_2 = \epsilon f(t_n + \frac{1}{2}\epsilon, y_n + \frac{1}{2}k_1) \tag{56}$$

$$k_3 = \epsilon f(t_n + \frac{1}{2}\epsilon, y_n + \frac{1}{2}k_2) \tag{57}$$

$$k_4 = \epsilon f(t_n + \epsilon, y_n + k_3) \tag{58}$$

the schemes for Euler, RK2 and RK4 can be summarized in Table 5. Note how complexity is built up in this scheme. For nonlinear ODEs this can lead to many terms involving powers and derivatives of the original variables, as discussed in Sec. 2.4.

In the subsections to follow, Δy will be computed in the RK2 scheme and then expanded with respect to ϵ . Since the FJet maps are models of Δy , this expansion essentially becomes a derivation of the models $h=(h_1,h_2,\dots)$ in the feature regression technique. In the examples to follow, $y=(u,\dot{u})$, and so

$$\Delta y = \begin{bmatrix} \Delta u \\ \Delta \dot{u} \end{bmatrix} = \begin{bmatrix} h_1 \\ h_2 \end{bmatrix}$$

Scheme	Δy_n	Accuracy
Euler	k_1	$O(\epsilon^2)$
RK2	k_2	$O(\epsilon^3)$
RK4	$\frac{1}{6}(k_1 + 2k_2 + 2k_3 + k_4)$	$O(\epsilon^5)$

Table 5: Update values Δy_n for three numerical integration schemes. Note the different level of accuracy in the time step ϵ .

where h_1 and h_2 are functions of (u, \dot{u}) .

Harmonic Oscillator (damped)

The equation of motion for a damped harmonic oscillator with natural frequency ω_0 and damping coefficient γ is

$$\ddot{u} = -\omega_0^2 u - 2\gamma \dot{u} \tag{59}$$

Writing $v = \dot{u}$, it is equivalent to

$$\begin{bmatrix} \dot{u} \\ \dot{v} \end{bmatrix} = \begin{bmatrix} v \\ -\omega_0^2 u - 2\gamma v \end{bmatrix} = f \begin{pmatrix} \begin{bmatrix} u \\ v \end{bmatrix} \end{pmatrix}$$

Note that there is no explicit time dependence in f. The RK2 scheme produces

$$\begin{bmatrix} h_1 \\ h_2 \end{bmatrix} = \epsilon \begin{bmatrix} v - \frac{\epsilon}{2}\omega^2 u - \epsilon \gamma v \\ -\omega_0^2 (u + \frac{\epsilon}{2}v) - 2\gamma (v - \frac{\epsilon}{2}\omega_0^2 u - \epsilon \gamma v) \end{bmatrix}$$
$$= \epsilon \begin{bmatrix} -\frac{\epsilon}{2}\omega_0^2 & 1 - \epsilon \gamma \\ -\omega_0^2 (1 - \epsilon \gamma) & -2\gamma (1 - \epsilon \gamma) - \frac{\epsilon}{2}\omega_0^2 \end{bmatrix} \begin{bmatrix} u \\ v \end{bmatrix}$$

This shows the how the vector $(u,v)^T$ naturally appears as the features. If RK4 were instead used, terms higher order in ϵ would appear in the matrix, but the set of features (i.e., $\{u,v\}$) would remain the same.

Pendulum (damped)

The equation of motion for the pendulum with natural frequency ω_0 is

$$\ddot{u} = -2\gamma \dot{u} - \omega_0^2 \sin u \tag{60}$$

After setting $v = \dot{u}$, it is equivalent to

$$\begin{bmatrix} \dot{u} \\ \dot{v} \end{bmatrix} = \begin{bmatrix} v \\ -2\gamma \dot{u} - \omega_0^2 \sin u \end{bmatrix} = f \begin{pmatrix} \begin{bmatrix} u \\ v \end{bmatrix} \end{pmatrix}$$

Note that there is no explicit time dependence in f. Then the RK2 scheme produces

$$\begin{bmatrix} h_1 \\ h_2 \end{bmatrix} = \epsilon \begin{bmatrix} (1 - \epsilon \gamma)v - \frac{\epsilon}{2}\omega_0^2 \sin u \\ -2\gamma(1 - \epsilon \gamma)v + \epsilon \gamma \omega_0^2 \sin u - \omega_0^2 \sin(u + \frac{\epsilon}{2}v) \end{bmatrix}$$
 (61)

$$= \epsilon \begin{bmatrix} (1 - \epsilon \gamma) & -\frac{\epsilon}{2} \omega_0^2 & 0\\ -2\gamma (1 - \epsilon \gamma) & -\omega_0^2 (1 - \epsilon \gamma) & -\frac{\epsilon}{2} \omega_0^2 \end{bmatrix} \begin{bmatrix} v\\ \sin u\\ v \cos u \end{bmatrix} + O(\epsilon^3)$$
 (62)

Thus, this expansion in ϵ produces a model akin to the feature regression technique, with the set of predictor variables: $\{v, \sin u, v\cos u\}$. If the RK4 were instead used, the reader would find this set to be

$$\{v, \sin u, v \cos u, v^2 \sin u, \sin u \cos u, v^3 \cos u, v \sin^2 u, v \cos^2 u\}$$

Note how these extra terms could arise from Eqn. 6.

Duffing Oscillator

The equation of motion for the Duffing oscillator is

$$\ddot{u} + 2\gamma \dot{u} + \alpha u + \beta u^3 = p(t) \tag{63}$$

where $p(t) = A \cos \Omega t$ and $\beta, \gamma > 0$. Writing $v = \dot{u}$, it is equivalent to

$$\begin{bmatrix} \dot{u} \\ \dot{v} \end{bmatrix} = f\left(t, \begin{bmatrix} u \\ v \end{bmatrix}\right) = \begin{bmatrix} v \\ -2\gamma v - \alpha u - \beta u^3 + p(t) \end{bmatrix}$$

Note that in this case there is explicit time dependence in f due to p(t). The RK2 scheme produces

$$\begin{bmatrix} h_1 \\ h_2 \end{bmatrix} = \epsilon \begin{bmatrix} (1 - \epsilon \gamma)v - \frac{\epsilon}{2}\alpha u - \frac{\epsilon}{2}\beta u^3 + \frac{\epsilon}{2}p(t) \\ -2\gamma(1 - \epsilon \gamma)v - \frac{\epsilon}{2}\alpha v - \alpha(1 - \epsilon \gamma)u + \epsilon\beta\gamma u^3 - \beta(u + \frac{\epsilon}{2}v)^3 - \epsilon\gamma p(t) + p(t + \frac{\epsilon}{2}) \end{bmatrix}$$

$$= \epsilon \begin{bmatrix} (1 - \epsilon \gamma) & -\frac{\epsilon}{2}\alpha & -\frac{\epsilon}{2}\beta & 0 & \frac{\epsilon}{2} & 0 \\ -2\gamma(1 - \epsilon \gamma) - \frac{\epsilon}{2}\alpha & -\alpha(1 - \epsilon \gamma) & -\beta(1 - \epsilon \gamma) & -\frac{3\epsilon}{2}\beta & (1 - \epsilon \gamma) & \frac{\epsilon}{2} \end{bmatrix} \begin{bmatrix} v \\ u \\ u^3 \\ u^2v \\ p \\ \dot{p} \end{bmatrix} + O(\epsilon^3)$$

where \dot{p} denotes the time derivative of p. Thus, this numerical integration scheme implies the vector of predictor variables $X=(v,u,u^3,u^2v,p,\dot{p})^T$ if feature regression is used.

General Expansion

Consider the above cases, where there is no explicit time dependence. In that case, the k_i can be written

$$k_{i+1} = \epsilon f\left(\begin{bmatrix} u + \delta u_i \\ v + \delta v_i \end{bmatrix}\right)$$

where i = 1, 2, 3 and k_1 is just ϵf . Now use subscripts a, b to identify the top (a) and bottom (b) components of the 2-by-1 vector:

$$\delta u_1 = (1,0) \left[\frac{1}{2} k_1 \right] \equiv (\frac{1}{2} k_1)_a = \frac{\epsilon}{2} f_a = \frac{\epsilon}{2} v$$

$$\delta v_1 = (0,1) \left[\frac{1}{2} k_1 \right] \equiv (\frac{1}{2} k_1)_b = \frac{\epsilon}{2} f_b = -\frac{\epsilon}{2} \sin u$$

Likewise,

$$\delta u_2 = (\frac{1}{2}k_2)_a$$

$$\delta v_2 = (\frac{1}{2}k_2)_b$$

$$\delta u_3 = (k_3)_a$$

$$\delta v_3 = (k_3)_b$$

Using the expression for k_{i+1} and expanding it with respect to δu_i and δv_i , and taking advantage of the fact that in this example many of the partial derivatives of f with respect to u,v are zero, one obtains

$$k_{i+1} = \epsilon \left\{ f + \delta u_i \partial_u f + \delta v_i \partial_v f + \frac{1}{2!} (\delta u_i)^2 \partial_u^2 f + \frac{1}{3!} (\delta u_i)^3 \partial_u^3 f + \dots \right\}$$

where $\partial_u f = \partial f/\partial u$, etc. This expansion is stopped at third order, because higher orders will lead to contributions beginning at $\mathcal{O}(\epsilon^5)$. These are ignored for the case of RK4 since it is an $\mathcal{O}(\epsilon^5)$ algorithm.

The point of doing this expansion is to demonstrate how low complexity models might be motivated from the standpoint of a numerical integration scheme. The above equation shows that all manner of monomials result, involving the original feature set and various derivatives and products of them. Also, keep in mind that the complexity builds on this, since k_1 gets substituted into k_2 , and then into k_3 and k_4 . It is this expansion which is the motivation for the guidance given in Eq. 6.

Appendix B: Stability – Harmonic Oscillator

The stability is now analyzed by focusing on a conserved quantity, the energy $E = \frac{1}{2}(u^2 + \dot{u}^2)$, where now $\omega_0 = 1$ and $\gamma = 0$. Following Young [2020], the energy at the nth step (E_n) may be expressed as

$$2E_n = r^{2n} = e^{(\log r^2)n} = e^{\lambda n}$$
 (64a)

$$r^2 = (1 + a_1)^2 + a_2^2 (64b)$$

where the initial condition of $(u, \dot{u}) = (1, 0)$ is used. Thus, the key quantity is $\lambda = \log r^2$; it measures the exponential growth/decay of E. Of course, the best choices for a_1, a_2 would lead to r = 1, so that $\lambda = 0$. Formulae for a_1, a_2 from Appendix A due to Euler/RK2/RK4 are given in Table 6. The values they lead to, along with the values for them due to the FJet method, are given in Table 7. Upon substituting these values into Eq.64b and computing $\lambda = \log(r^2)$, the values for Table 2 are produced.

Appendix C: Derivation of r **for Damped Oscillator**

Rather than working directly on

	Euler	RK2	RK4
$\overline{a_1}$	0	$-\epsilon^2/2$	$-\epsilon^2/2 + \epsilon^4/24$
a_2	ϵ	ϵ	$\epsilon - \epsilon^3/6$

Table 6: Values for a_1 , a_2 for the Euler/RK2/RK4 integration schemes.

	Euler	RK2	RK4	FJet
$\overline{a_1}$	0	-0.005	$-0.00499583\bar{3}$	-0.004995834721974124
a_2	0.1	0.1	$0.09983\bar{3}$	0.09983341664682731

Table 7: Values for a_1 , a_2 using $\epsilon = 0.1$ for the Euler/RK2/RK4 schemes, based on expressions from Table 6. Also included are the values for the FJet method.

where

$$A = \begin{bmatrix} 0 & 1 \\ -\omega_0^2 & -2\gamma \end{bmatrix}$$

the approach will be to first transform A. It is diagonalized as $A=S\Lambda S^{-1},$ where

$$S = \begin{bmatrix} 1 & 1 \\ \lambda_{+} & \lambda_{-} \end{bmatrix}$$

$$\Lambda = \begin{bmatrix} \lambda_{+} & 0 \\ 0 & \lambda_{-} \end{bmatrix}$$

$$S^{-1} = \frac{1}{2} \begin{bmatrix} 1 - i\gamma/\omega & -i/\omega \\ 1 + i\gamma/\omega & i/\omega \end{bmatrix}$$

where $\lambda_{\pm} = -\gamma \pm i\omega$. Upon defining

$$\begin{bmatrix} \bar{u} \\ \bar{v} \end{bmatrix} = S^{-1} \begin{bmatrix} u \\ v \end{bmatrix}$$

and similarly for du, dv, Eq. 65 becomes transformed to

$$\begin{bmatrix} d\bar{u} \\ d\bar{v} \end{bmatrix} = \Lambda \begin{bmatrix} \bar{u} \\ \bar{v} \end{bmatrix} \epsilon$$

Following the approach of Sec. 2.5, the constant of motion is found through integration to be

$$r = \gamma \ln \left(\frac{\bar{u}}{\bar{v}}\right) + i\omega \ln \left(\bar{u}\bar{v}\right)$$

where

$$\begin{split} \bar{u} &= a - ib \\ \bar{v} &= a + ib \\ a &= u/2 \\ b &= (\gamma u + v)/(2\omega) \end{split}$$

$$r = \ln \left[\frac{1}{2}\omega^2 u^2 + \frac{1}{2}(\gamma u + v)^2 \right] + \frac{2\gamma}{\omega}\phi_n - \ln(2\omega^2)$$

with $\tan \phi_n = -b/a$. The constant term $\ln(2\omega^2)$ is not needed and will be dropped.

References

- H. Poincaré. Sur les courbes définies par une équation différentielle. *Journal de Mathématiques Pures et Appliquées*, 4(1):167–244, 1885.
- P. Holmes. Poincaré, celestial mechanics, dynamical-systems theory and "chaos". *Physics Reports*, 193(3):137–163, 1990.
- H. Poincaré. New Methods of Celestial Mechanics, 1: Periodic and Asymptotic Solutions (Ed. D.L. Goff). American Institute of Physics, 1993.
- N.H. Packard, J.P. Crutchfield, J.D. Farmer, and R.S. Shaw. Geometry from a time series. *Physical Review Letters*, 45, 1980.
- F. Takens. Detecting strange attractors in turbulence. In *Lecture Notes in Mathematics: Dynamical Systems and Turbulence, Warwick 1980 (Coventry, 1979/1980)*, volume 898, pages 366–381. Springer, 1981.
- J.P. Crutchfield and B.S. McNamara. Equations of motion from a data series. *Complex Systems*, 1:417–452, 1987.
- D.S. Broomhead and D. Lowe. Multivariable functional interpolation and adaptive networks. *Complex Systems*, 2(3):321–355, 1988.
- M. Casdagli. Nonlinear prediction of chaotic time series. *Physica D*, 35(3):335–356, 1989.
- J. Cremers and A. Hübler. Construction of differential equations from experimental data. *Zeitschrift für Naturforschung A*, 42(8):797–802, 1987.
- J.L. Breeden and A. Hübler. Reconstructing equations of motion from experimental data with unobserved variables. *Physical Review A*, 42, 1990.
- G. Gouesbet. Reconstruction of vector fields: the case of the lorenz system. *Physical Review A*, 46(4):1784–1796, 1992.
- L.A. Aguirre and C. Letellier. Modeling nonlinear dynamics and chaos: A review. *Mathematical Problems in Engineering*, 2009, 2009.
- M. Lutter, C. Ritter, and J. Peters. Deep Lagrangian Networks: Using physics as model prior for deep learning. In *International Conference on Learning Representations* (*ICLR*), 2019.
- M. Cranmer, S. Greydanus, S. Hoyer, P. Battaglia, D. Spergel, and S. Ho. Lagrangian neural networks. *arXiv preprint*, arXiv:2003.04630, 2020.

- S. Greydanus, M. Dzamba, and J. Yosinski. Hamiltonian neural networks. In *Neural Information Processing Systems (NeurIPS)*, pages 15353–15363, 2019.
- P. Toth, D.J. Rezende, A. Jaegle, S. Racanière, A. Botev, and I. Higgins. Hamiltonian generative networks. volume arXiv:1909.13789, 2019.
- S.H. Rudy, S.L. Brunton, J.L. Proctor, and J.N. Kutz. Data driven discovery of partial differential equations. *Science Advances*, 3(4), 2017.
- Z. Liu, B. Wang, Q. Meng, W. Chen, M. Tegmark, and T.-Y. Liu. Machine-learning non-conservative dynamics for new-physics detection. arXiv preprint, arXiv:2106.00026, 2021.
- P.E. Hydon. Symmetry Methods for Differential Equations: A Beginner's Guide. Cambridge, 2000.
- P.J. Olver. Applications of Lie Groups to Differential Equations. Springer-Verlag, 2nd edition, 1993.
- T. Hastie, R. Tibshirani, and J. Friedman. *The Elements of Statistical Learning: Data Mining, Inference, and Prediction.* Springer-Verlag, 2nd edition, 2009.
- G.W. Bluman and S. Kumei. *Symmetries and Differential Equations*. Springer-Verlag, 1989.
- A.P. Young. Physics 115/242, Comparison of methods for integrating the simple harmonic oscillator, 2020. URL https://young.physics.ucsc.edu/115/ode_solve.pdf.
- G. Duffing. Erzwungene schwingungen bei veränderlicher eigenfrequenz und ihre technische bedeutung [Forced oscillations with variable natural frequency and their technical relevance]. *Vieweg, Braunschweig*, 41/42, 1918.
- F.C. Moon and P.J. Holmes. A magnetoelastic strange attractor. *Journal of Sound and Vibration*, 65:275–296, 1979.
- E.A. Jackson. *Perspectives of nonlinear dynamics*, volume 1. Cambridge University Press, 1991.
- W.H. Press, S.A. Teukolsky, W.T. Vetterling, and B.P. Flannery. *Numerical Recipes*, *The Art of Scientific Computing*. Cambridge University Press, 3rd edition, 2007.